Effect of braking torque on vehicle nonlinear dynamics

Xianbin Wang (xbwang10@163.com)
Northeast Forestry University https://orcid.org/0000-0002-0035-5616
Weifeng Li
Northeast Forestry University
Zhipeng Li
Northeast Forestry University
Zexuan Li
Northeast Forestry University
Fugang Zhang
Northeast Forestry University

Research Article

Keywords: Nonlinear dynamics, Braking torque, Phase space analysis, Bifurcation analysis, Chaos analysis

Posted Date: June 2nd, 2022

DOI: https://doi.org/10.21203/rs.3.rs-1672886/v1

Effect of braking torque on vehicle nonlinear dynamics

Xianbin Wang Weifeng Li Zhipeng Li Zexuan Li Fugang Zhang

(Traffic College, Northeast Forestry University, Harbin 150040, China.)

Corresponding author: Xianbin Wang

(Email:xbwang10@163.com)

Abstract: To analyze the effect of braking torque on vehicle nonlinear dynamic characteristics, a five-degree-of-freedom(5DOF) vehicle nonlinear dynamic model including braking torque is established in this paper. The global dynamic characteristics of the model are analyzed through the phase space of multiple initial points. The effect of constant braking torque on vehicle dynamic characteristics is studied by time-domain analysis and tire force distribution characteristics of a single initial point. The characteristics of bifurcation and chaos are analyzed by using the differences in trajectories in phase space, the bifurcation diagram of state variables and the Lyapunov exponent spectrum. The results show that the braking torque has a significant impact on the vehicle's nonlinear dynamic characteristics; With the increase of the braking torque, the five-degree-of-freedom model system may occur multiple bifurcations and hyperchaos under the condition of the zero-steering angle of the front wheel; some instable vehicle dynamic states under zero front-wheel steering angle can only be restored to a stable state with the action of braking torque in a certain range of values.

Keywords*: Nonlinear dynamics· Braking torque· Phase space analysis ·Bifurcation analysis· Chaos analysis*

1 Introduction

As a typical nonlinear dynamic system, the vehicle is prone to exhibit unstable dynamic behaviours under extreme working conditions, accompanied by nonlinear characteristics such as bifurcation and chaos. At present, the vehicle steering bifurcation instability mechanism based on the nonlinear characteristics of tire lateral force has been confirmed[1-3], and both simple and extremely complex bifurcations may occur when different combinations of front and rear tire characteristics are considered[4]. Based on the two-degree-of-freedom model and its extension, the research of control strategy has achieved fruitful results[5,6], which effectively improves the handling and stability of the vehicle. However, the two-degree-of-freedom model assumes that the longitudinal velocity is constant, and does not consider the influence of the longitudinal tire force on the system stability. The steering bifurcation mechanism of the parameters cannot fully explain the dynamic bifurcation characteristics of the vehicle under the combined working conditions of driving or braking and steering.

A three-degree-of-freedom model has been proposed in [7] by introducing the longitudinal velocity into the vehicle body model based on the two-degree-of-freedom model, discovering the chaotic phenomenon of vehicle steering motion, and pointing out that the essential feature of vehicle steering instability is the chaotic motion of the vehicle dynamic system. Based on the three-degree-of-freedom model, the five-degree-of-freedom considers the rotation of the wheel and introduces the driving torque, analyzed the effect of driving

mode on vehicle stability under different steering angles[8], and two-dimensional bifurcation parameter set (driving stability region) and coupling bifurcation characteristics were obtained in the later research[9,10]. A novel control algorithm of DYC based on the hierarchical control strategy is brought forward in [11] and effectively improved the vehicle's stability. The relationship between tire slip rate and stability region during steering braking and steering acceleration is analyzed in the [12]. To extend the limit of vehicle cornering stability, a new method for integrating sideslip control into a continuous yaw rate controller is proposed in [13]. For the enhanced nonlinear vehicle model,When a human driver controls a vehicle through the steering, it has been shown that the driver may affect the stability of the system, depending on the available preview distance in front of the vehicle [14]. The existence of Hopf bifurcation in the straight-line driving stability of the vehicle through the driving simulator test have found in [15]. The study in [16] enhances the directional stability of a vehicle that turns at high speeds on various road conditions using integrated active steering and differential braking systems. The application of phase diagrams in vehicle dynamics has extended to control synthesis by showing how open-loop vehicle dynamics can be increased by steering and braking through closed-loop phase diagrams[17]. The Small-amplitude limit cycles close to the Hopf bifurcation point emerge with the steering angle (drive torque) as a bifurcation parameter[18], followed by large amplitude relaxation cycles. The research in [19] shows that rear-wheel-drive vehicles and front-wheel drive vehicles show different behaviours by using bifurcation analysis, especially when approaching their handling limit.

From the above studies, it can be found that the research on vehicle steering bifurcation based on steering angle and the bifurcation characteristics of driving torque as a control parameter is relatively complete, but the braking torque, also as a control parameter, has been little studied for the dynamic characteristics and stability of the vehicle. Meanwhile in longitudinal motion control in the field of autonomous driving, most longitudinal motion control studies involve relatively simple vehicle conditions and therefore rarely take into account the nonlinear characteristics of the tires, the longitudinal-lateral coupling characteristics of the vehicle under large lateral accelerations, and the effects of tire force constraints [20]. By studying the vehicle model with the introduction of braking torque, considering the nonlinear factors of the vehicle under extreme working conditions and the mechanism of the longitudinal lateral coupling characteristics of the tire on the longitudinal control, and establishing a vehicle dynamics model with longitudinal and lateral tire force coordination mechanism, it is of great significance to ensure the driving stability of the vehicle.

Therefore, a 5DOF nonlinear dynamic model of a vehicle system including braking torque in-plane motion is established in this paper, and then the global dynamic characteristics of the vehicle system are analyzed through phase space, and the influence of constant braking torque on vehicle dynamic characteristics under zero front-wheel steering angle is analyzed. On this basis, the bifurcation diagram of the system state variables with different braking torques and the Lyapunov exponent spectrum at the bifurcation point is calculated. Finally, a conjecture is put forward according to the phenomenon of the bifurcation diagram and verified.

2 5DOF System Model

2.1 Vehicle model

Fig. 1 and Fig. 2 show diagrams of the single-track model and the single-wheel braking model respectively.

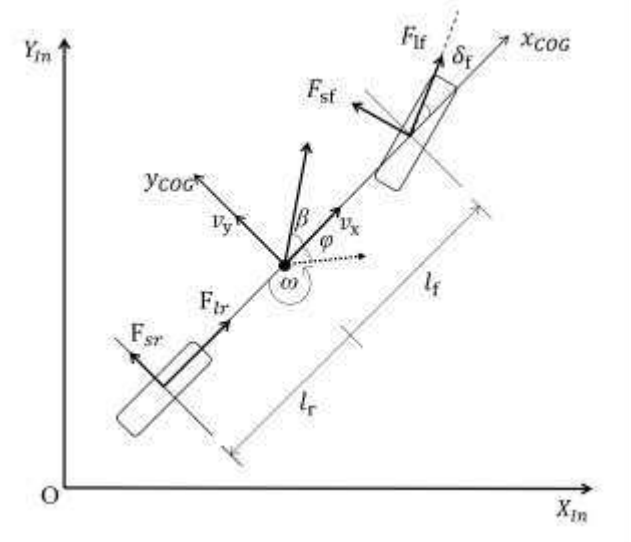

Fig. 1 the single-track model diagram

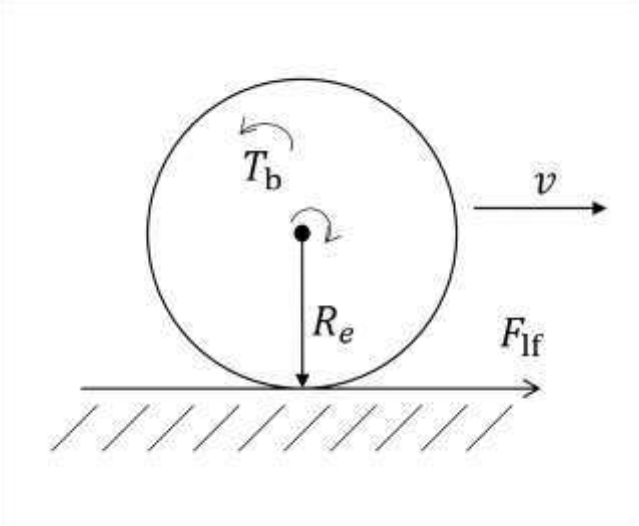

Fig. 2 the single-wheel braking model diagram

Based on the three-degree-of-freedom vehicle steering system model in [7], considering the air resistance of the vehicle body, the wheel rotation equation including braking torque is introduced, and the five-degree-of-freedom vehicle dynamics system equation is obtained as follows:

$$\begin{cases} \overset{g}{v_y} = -v_x\omega + \dfrac{F_{lf}\sin\delta_f + F_{sf}\cos\delta_f + F_{sr} - \mathrm{sgn}(v_y)\cdot C_{air\_y}A_{L\_y}\dfrac{\rho}{2}v_y^{\,2}}{m} \\ \overset{g}{\omega} = \dfrac{(F_{lf}\sin\delta_f + F_{sf}\cos\delta_f)l_f - F_{sr}l_r}{I_z} \\ \overset{g}{v_x} = v_y\omega + \dfrac{F_{lf}\cos\delta_f - F_{sf}\sin\delta_f + F_{lr} - \mathrm{sgn}(v_x)\cdot C_{air\_x}A_{L\_x}\dfrac{\rho}{2}v_x^{\,2}}{m} \\ \overset{g}{\omega_f} = \dfrac{-\mathrm{sgn}(\omega_f)\cdot T_{bf} - R_e\cdot\dfrac{F_{lf}}{2}}{J\omega} \\ \overset{g}{\omega_r} = \dfrac{-\mathrm{sgn}(\omega_r)\cdot T_{br} - R_e\cdot\dfrac{F_{lr}}{2}}{J\omega} \end{cases} \tag{1}$$

where m is the mass of the vehicle, I_z is the yaw moment of inertia of the vehicle, v_x is the longitudinal velocity, v_y is the lateral velocity, ω is the yaw rate, ω_f is the angular velocity of the front wheel, ω_r is the angular velocity of the rear wheel, l_f is the distance from the front axle to the mass centre, l_r is the distance from the rear axle to the mass centre, J is the yaw moment of inertia of the wheels, δ_f is the front wheel steering angle, C_{air_x} is the longitudinal air resistance coefficient, C_{air_y} is the lateral air resistance coefficient, A_{L_x} is the longitudinal area of the vehicle, A_{L_y} is the lateral area of the vehicle, ρ is the density of air, T_{bf} is the braking torque of the front wheel, T_{br} is the braking torque of the rear wheel, R_e is the rolling radius of the wheel, F_{lf} and F_{lr} are the longitudinal tire forces of the front wheel and the rear wheel respectively, F_{sf} and F_{sr} are the lateral tire forces of the front wheel and the rear wheel respectively.

This paper regards braking torque T_b as a positive scalar to facilitate research and description.

To prevent the rear wheel from locking up first and causing a sideslip during braking, the braking torque will be applied mainly to the front wheel and distributed between the front and rear wheel according to the following formula.

$$\begin{cases} T_{bf} = \eta T_b \\ T_{br} = (1-\eta) T_b \end{cases} \tag{2}$$

Where η is the distribution factor of the braking torque, T_b is the total braking torque of the front and rear wheels.

Braking torque T_b is applied in such a way that the maximum braking force applied to the wheels does not exceed the maximum traction available from the road surface.

$$\max T_b = \mu m g R_e \tag{3}$$

Where μ is the road adhesion coefficient(In this study, a low road adhesive coefficient is selected).

The specific parameters values for the vehicle system model are shown in Table 1.

Table 1 Vehicle system model parameters

Parameters	Values
m/kg	1500
I_z/(kg·m^2)	3000
l_f/m	1.2
l_r/m	1.3
J/(kg·m^2)	2
C_{air_x}	0.3
C_{air_y}	0.4
A_{L_x}/m^2	1.7
A_{L_y}/m^2	3.5
ρ/(kg·m^3)	1.2258
R_e/m	0.224

μ	0.3
η	0.7

2.2 Tire model

The tire force is modelled by the Magic Formula[22].

$$F = D\sin\left(C\arctan\left(Bx - E\left(Bx - \arctan Bx\right)\right)\right) \tag{4}$$

where B, C, D, and E are coefficients. F is the longitudinal or lateral tire force, and x is the longitudinal slip or sideslip angle.

Longitudinal slip k is calculated using the uniform tire longitudinal slip formula at full working conditions[8].

$$k = \frac{\omega_w R_e - v_{wx}}{|v_{wx}|} \tag{5}$$

Where ω_w is the angular velocity of the wheel, and v_{wx} is the linear velocity at the wheel centre in the longitudinal direction.

The sideslip angles of the front and rear tire are calculated that introduce a symbolic function in the following[21]:

$$\begin{cases} \alpha_f = \left(\delta_f - \arctan\left(\dfrac{v_y + \omega l_f}{v_x}\right)\right)\cdot \mathrm{sgn}\left(v_{xf}\right) \\ \alpha_r = \left(-\arctan\left(\dfrac{v_y - \omega l_r}{v_x}\right)\right)\cdot \mathrm{sgn}\left(v_{xr}\right) \end{cases} \tag{6}$$

$$\begin{cases} \mathrm{v}_{xf} = v_x \cdot \cos\delta_f + (v_y + l_f \cdot \omega)\cdot \sin\delta_f \\ v_{xr} = v_x \end{cases} \tag{7}$$

Where α_f and α_r are the sideslip angle of the front and rear wheel respectively, v_{xf} is the longitudinal velocity of the front wheel in the tire coordinate system, and v_{xr} is the longitudinal velocity of the rear wheel in the tire coordinate system.

The tire force parameters used in the model are shown in Table 2 and Table 3.

Table 2 Longitudinal tire parameters

Tire	Value of the following coefficients			
	B	*C*	*D*	*E*
Front tire	11.275	1.56	2574.8	0.4109
Rear tire	18.631	1.56	1749.6	0.4108

Table 3 Lateral tire parameters

Tire	Value of the following coefficients

	B	*C*	*D*	*E*
Front tire	11.275	1.56	2574.7	-1.999
Rear tire	18.631	1.56	1749.7	-1.7908

By using models proposed by Pacejka[22], the combined slip characteristics, and the tire forces can be calculated as follow:

$$\begin{cases} F_{lf} = F_{lf0} \cdot G_x \\ F_{lr} = F_{lr0} \cdot G_x \\ G_x = \cos[\arctan\{B_{g,x}(\alpha) \cdot \alpha\}] \\ B_{g,x}(\alpha) = r_{x,1} \cos[\arctan(r_{x,2} \cdot k)] \\ F_{sf} = F_{sf0} \cdot G_y \\ F_{sr} = F_{sr0} \cdot G_y \\ G_y = \cos[\arctan\{B_{g,x}(k) \cdot k\}] \\ B_{g,y}(k) = r_{y,1} \cos[\arctan(r_{y,2} \cdot \alpha)] \end{cases} \tag{8}$$

G_x and G_y are the weighting functions for the tire forces, $B_{g,x}$ and $B_{g,y}$ are the shape functions for the tire slip and $r_{x,1}$,$r_{x,2}$,$r_{y,1}$ and $r_{y,2}$ are the combined slip coefficients, The best interactive curves are produced using the parameters in Table 4.

Table 4 Combined slip correction coefficient

Longitudinal slip coefficients		Lateral slip coefficients	
$r_{x,1}$	$r_{x,2}$	$r_{y,1}$	$r_{y,2}$
35	40	40	35

2.3 Validation

In the following two groups of experiments, the validity of the model is verified by the time-domain responses of single initial points and vehicle body postures.

Table 5 Model validation experimental conditions

Experimental groups	δ_f (rad)	v_x (m/s)	v_y (m/s）	ω （rad/s）	T_b （N·m）
First group	0	20 30 40	2	0.1	500
Second group	0.005 0.010 0.015	30	0	0	200

The first group is the experimental conditions under zero input of the front wheel steering angle. According to experience, vehicles with an initial longitudinal velocity from small to large will gradually decelerate to stop at the same braking torque, and the driving distance will also get longer. The second group is the experimental conditions for the fixed front wheel steering angle. Results show that vehicles with a large initial front-wheel steering angle will have a large radius in steering, and will decelerate until they stop under

the action of braking torque. However, it is not ruled out that vehicles will become unstable due to the large steering angle.

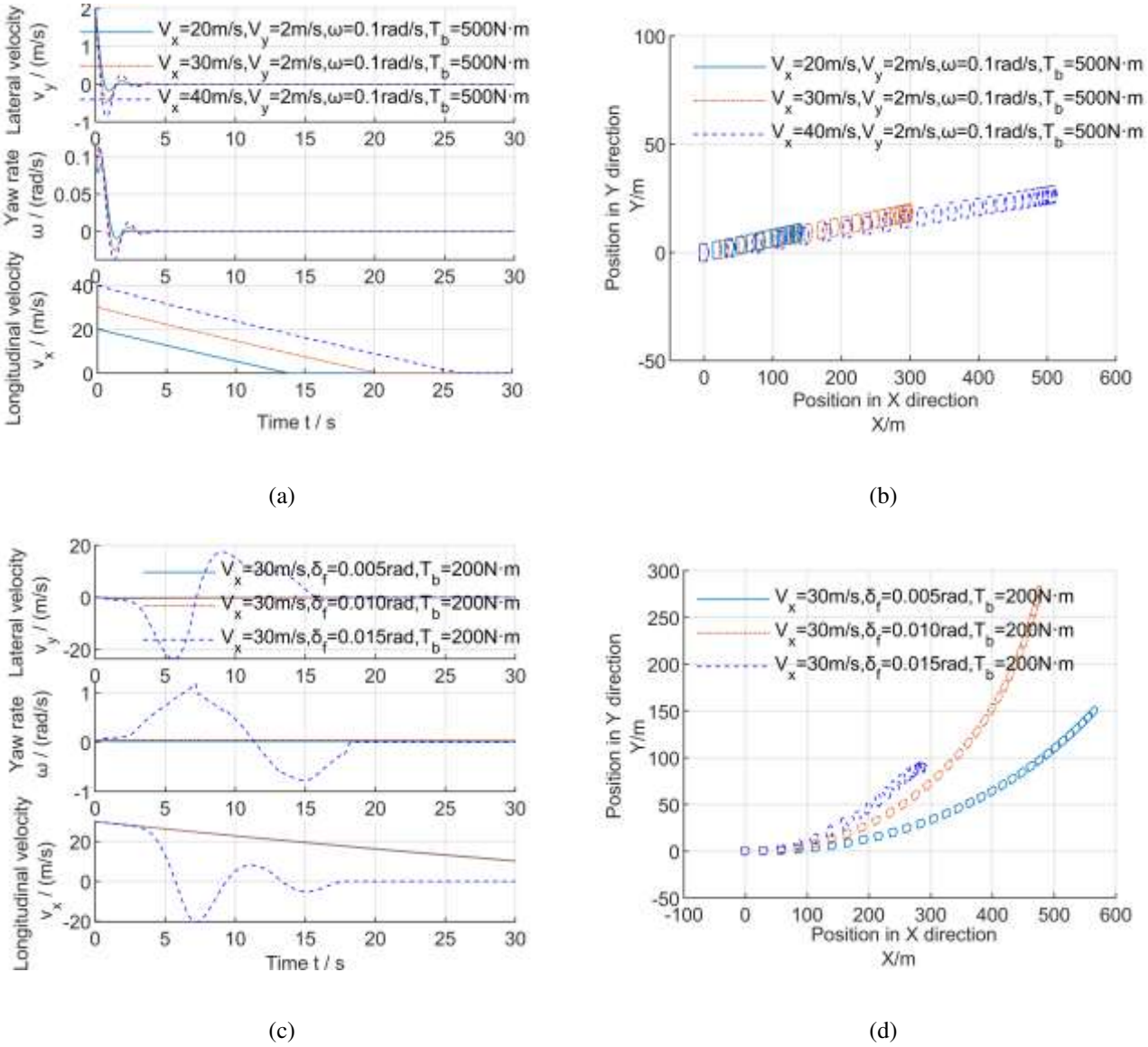

Fig. 3 Time-domain responses of single initial points and vehicle body postures of two experimental groups

Fig. 3 shows the simulation results under two experimental conditions. In the first group of experiments, the lateral velocity v_y and yaw rate ω of the vehicle system converges rapidly to 0, and the different longitudinal velocities v_x decrease linearly under the braking torque T_b until they reach 0. The body posture is stable in the body posture diagram (the pointed end represents the head). The distance between the two body postures decreases until they coincide, indicating that the vehicle is finally stationary.

In the second group of experiments, when the front wheel steering angles are $\delta_f = 0.005$rad and $\delta_f = 0.01$rad, the lateral velocity v_y and yaw rate ω are always close to 0, and the longitudinal velocity v_x decreases linearly under the action of braking torque. It can be seen in the body posture diagram that the vehicle is in steady-state steering, and the turning radius decreases in turn. The distance between the body postures

decreases continuously indicating that the vehicle will finally reach a standstill. However, when the front wheel steering angle is $\delta_f = 0.015$rad, the state variable of the vehicle fluctuates violently in the range of positive and negative values, indicating that the vehicle is in an unstable state at the beginning.

From the above analysis, it can be found that the 5DOF braking model can reflect the motion process of the vehicle under pure braking conditions and combined steering braking conditions. It can be used as a basic analysis model for studying the effect of braking torque on the dynamic characteristics of the vehicle system.

3 Phase space and time domain-analysis

3.1 Phase space analysis

Phase space characteristics are important research contents in nonlinear systems, and the vehicle moving process can be described by the movement process of phase points in phase space. By understanding the phase trajectory characteristics, the global motion views of multi-degree-of-freedom dynamic systems under different initial conditions can be obtained.

The simulations are under the condition of constant braking torque, and the value of the front wheel steering angle is $\delta_f = 0$. The specific stimulation parameters are as follows: the braking torques are $T_b = 0$N·m, $T_b = 500$N·m and $T_b = 1000$N·m respectively, the initial value of longitudinal velocity is $v_x = 42$m/s, the value ranges of lateral velocity v_y and yaw rate ω are [-10,10] m/s and [-1,1] rad/s respectively, the value intervals are 1m/s and 0.1rad/s, and the simulation time is 8s.

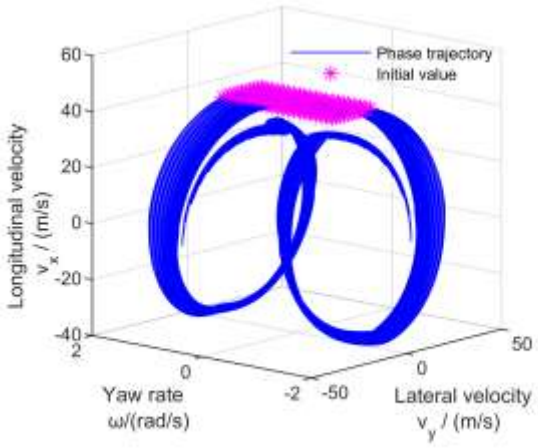

(a) $T_b = 0$N·m

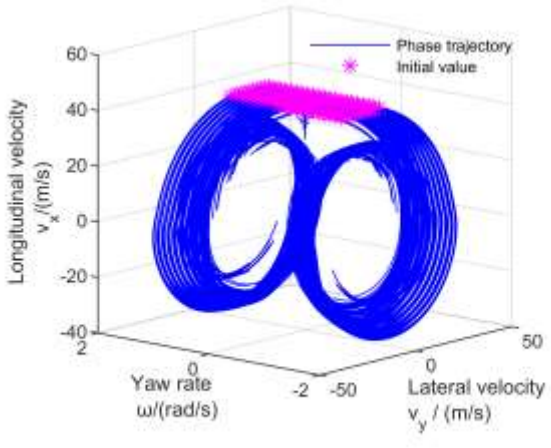

(b) $T_b = 500$N·m

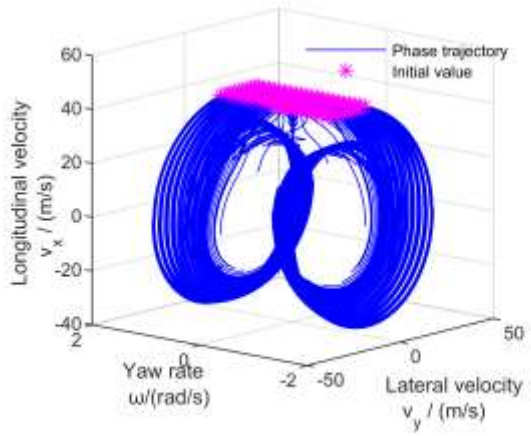

(c) T_b = 1000N·m

Fig. 4 Phase space trajectories with different braking torques

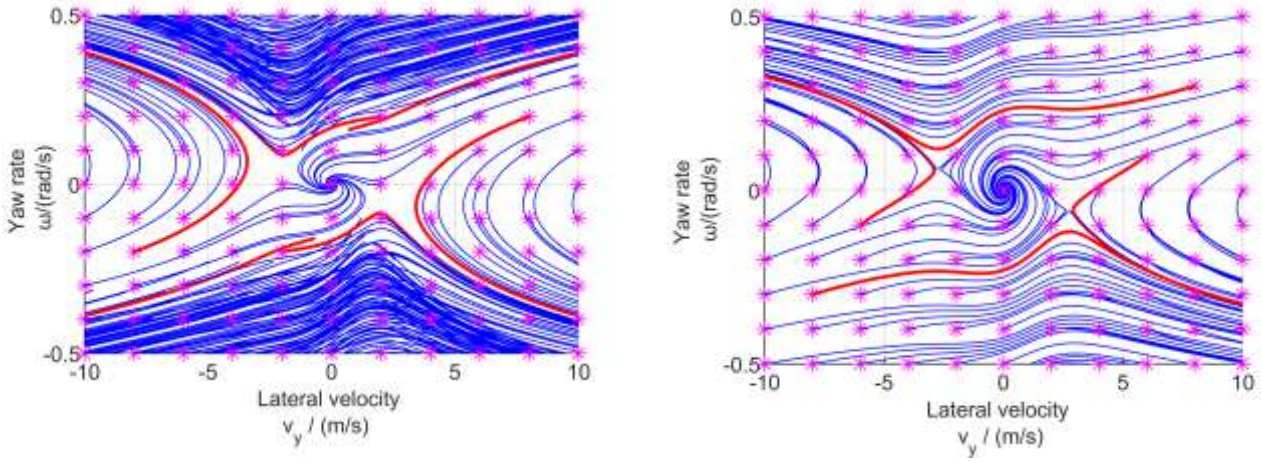

(a) T_b = 0N·m

(b) T_b = 500N·m

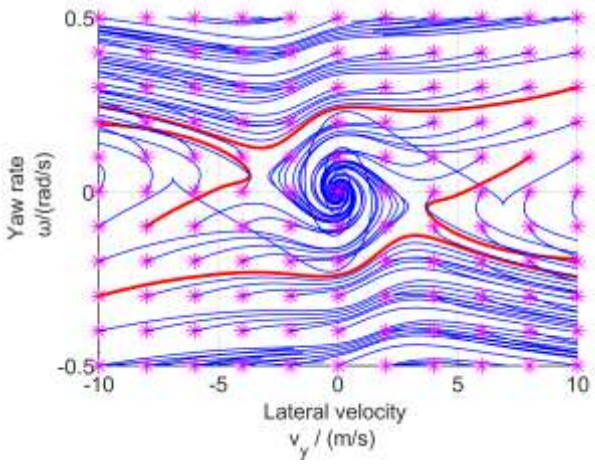

(c) T_b = 1000N·m

Fig. 5 Local phase trajectories onto the v_y-ω plane with different braking torques

The phase space trajectories of multiple initial points are shown in Fig. 4, and the local phase trajectories onto the v_y-ω plane are shown in Fig. 5. It can be seen from Fig. 4 that when the braking torque T_b is not applied to the vehicle system, the phase trajectory of the system is closely distributed, and the attenuation of longitudinal velocity is small. A clear banded stable region, namely the basin of attraction (the region surrounded by the red line in Fig. 5, can be seen in the v_y-ω plane). With the application and increase of braking torque, the phase trajectories of the system are gradually getting sparse, the longitudinal velocity attenuation is large, and the banded stability region increases accordingly. The differences in phase diagrams with braking torque application and without braking torque application represent the changes in dynamic characteristics of the system.

3.2 Time-domain analysis

The following is an analysis of the initial state of the vehicle, that is, a trajectory in phase space. Reducing the value interval of braking torque. The experimental conditions are as follows: the front wheel steering angle is $\delta_f = 0$, the braking torque is taken as $T_b = 250\text{N}\cdot\text{m}$, $T_b = 500\text{N}\cdot\text{m}$, $T_b = 750\text{N}\cdot\text{m}$ and $T_b = 1000\text{N}\cdot\text{m}$ respectively, the initial value of longitudinal velocity is $v_x = 42\text{m/s}$, the initial value of lateral velocity is $v_y = 4\text{m/s}$, the initial value of yaw rate is $\omega = 0.25\text{rad/s}$, and the simulation time is the 20s. The time-domain responses of state variables and vehicle body postures under different braking torques are shown in Fig. 6.

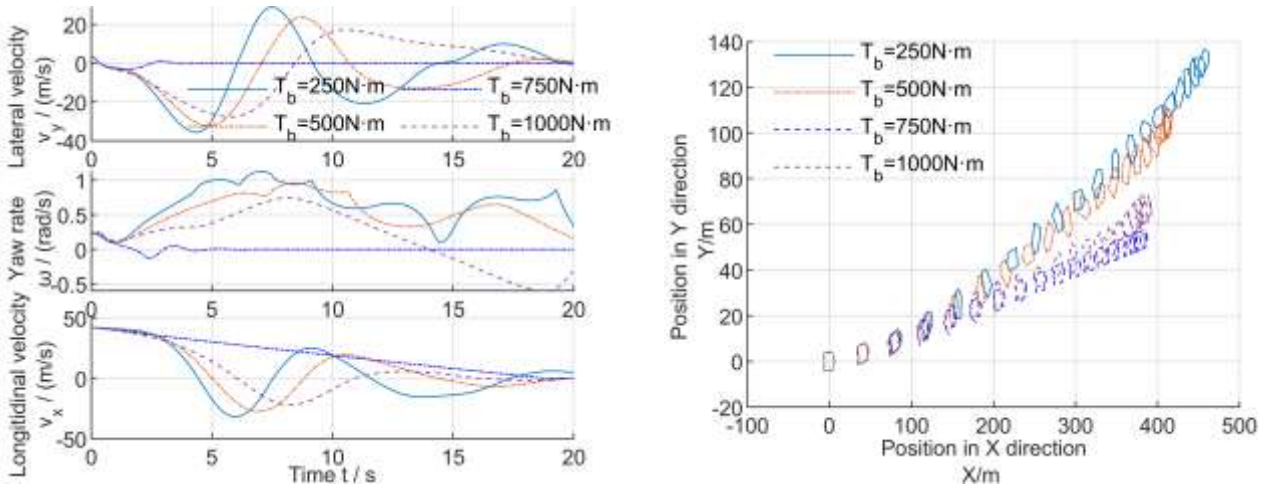

(a) (b)

Fig. 6 Time-domain responses of single initial points and vehicle body postures with different braking torques

When the braking torque is $T_b = 750\text{N}\cdot\text{m}$, the dynamic state of the vehicle system quickly recovers to stability. The lateral velocity v_y and yaw rate ω converge to 0, and the longitudinal velocity v_x decreases linearly to 0 under the action of constant braking torque. The body posture remains relatively stable during braking without unstable posture such as rotation.

However, when the braking torques are $T_b = 250\text{N}\cdot\text{m}$, $T_b = 500\text{N}\cdot\text{m}$ and $T_b = 1000\text{N}\cdot\text{m}$, the dynamic state of the vehicle system cannot be stable at the beginning. The lateral velocity v_y, yaw rate ω and longitudinal

velocity v_x fluctuate violently, and the change amplitudes are large. The vehicle's body posture starts to rotate at the beginning, indicating that the vehicle is unstable at this time.

It can be seen in Fig. 7 that when the braking torque is T_b = 750N·m, the longitudinal and lateral tire force stays in the linear region, but with other braking torques, the tire forces of the front and rear wheel transit from the linear region to the nonlinear region.

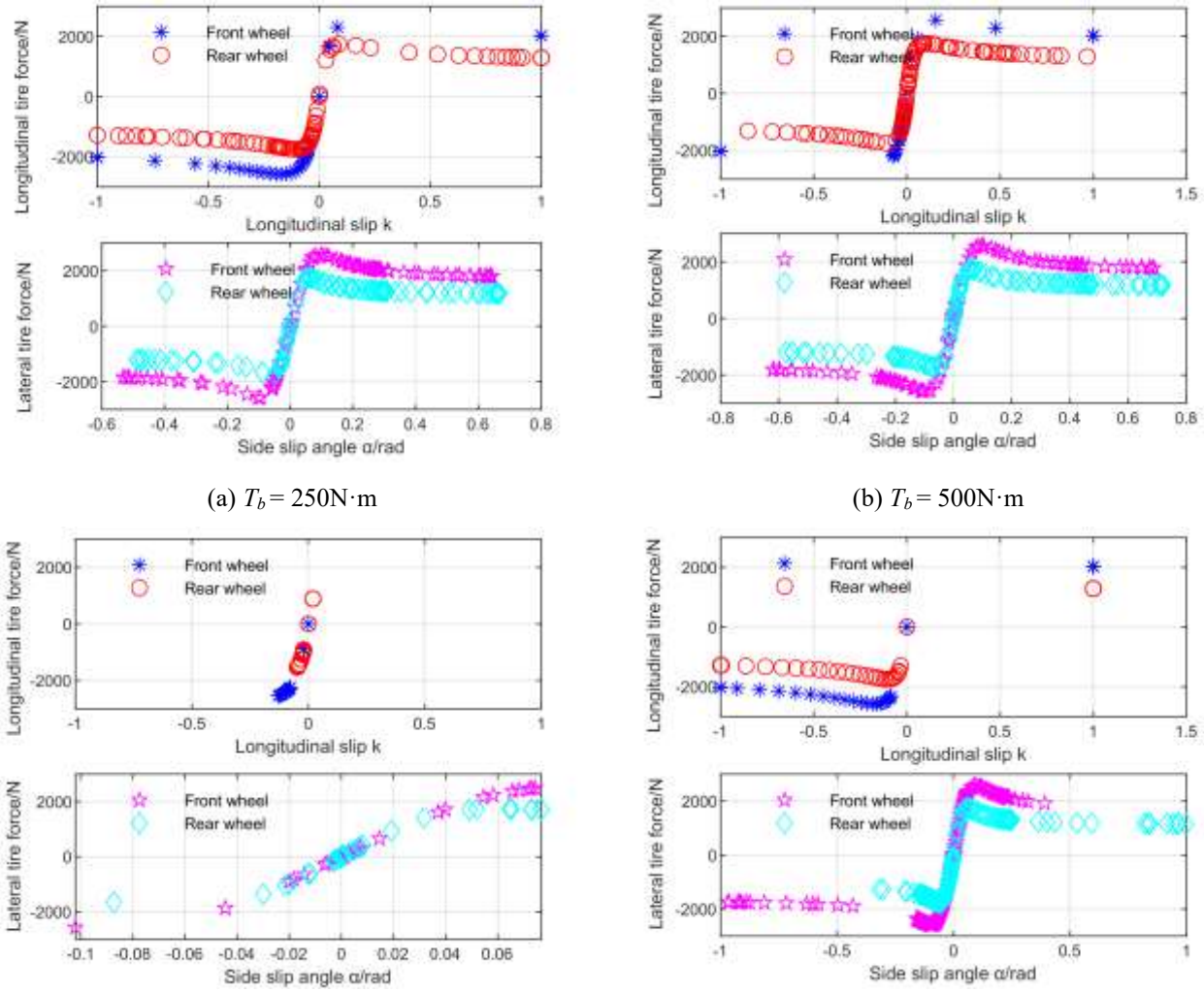

(a) T_b = 250N·m

(b) T_b = 500N·m

(c) T_b = 750N·m

(d) T_b = 1000N·m

Fig. 7 Tire forces distribution characteristics with different braking torques

From the above analysis, it is easy to know that when the vehicle loses stability, the tire force presents strong nonlinear characteristics, so that under the conditions of large lateral velocity and braking, the tire cannot provide enough longitudinal and lateral force to maintain the stable state of the vehicle. With the increase of braking torque T_b, the state of the vehicle system corresponds to an unstable state, a stable state and then an unstable state. Therefore, the braking torque T_b can be used as the analysis parameter of a nonlinear vehicle dynamics system to analyze the change in system state.

4 Bifurcation and Chaos

4.1 Bifurcation analysis

Using the definition of bifurcation of the nonlinear system [23], taking the braking torque T_b as the bifurcation parameter, the dynamic bifurcation characteristics of the 5DOF vehicle system are studied.

The phase space trajectories and phase trajectories onto the v_y-ω plane with different braking torques are shown in Fig. 8. The experimental conditions are as follows: the front wheel steering angle is $\delta_f = 0$, the value range of braking torque T_b is [650,700] N·m, the value interval is 10N·m, the initial value of longitudinal velocity is v_x = 42m/s, the initial value of lateral velocity is v_y =4m/s, the initial value of yaw rate is ω = 0.25rad/s, and the simulation time is 10s.

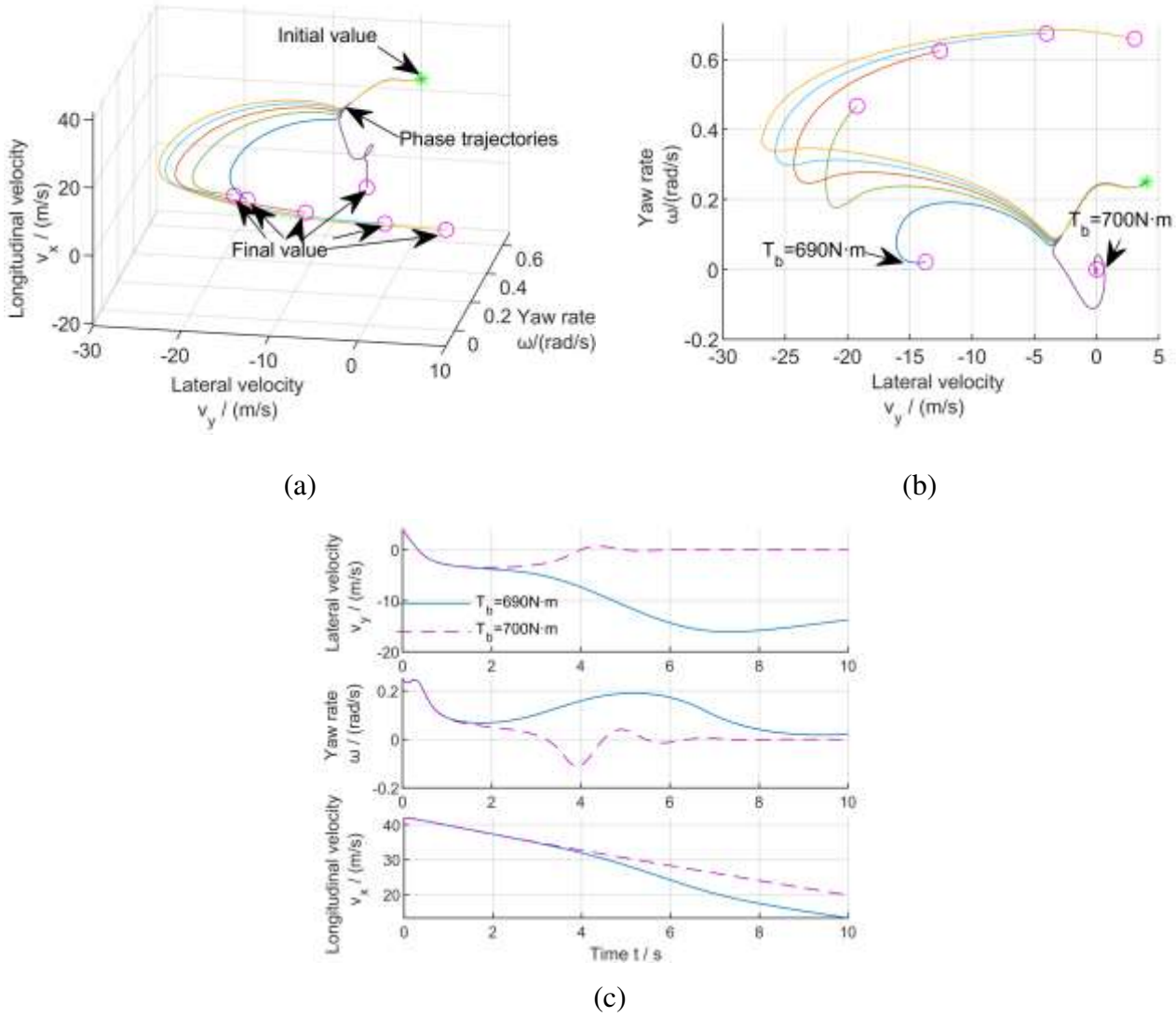

Fig. 8 Phase trajectories and time-domain responses of braking torques varying from 650N·m to 700N·m

Fig. 8 shows that the phase trajectories of the system change continuously with the increase of braking torque. When the braking torque increases from T_b = 690N·m to T_b = 700N·m, the phase trajectory of the system changes obviously in topology [23], that is, bifurcation occurs. From the time-domain response of state variables, it can be seen that the nature of the system solution has also changed essentially.

Continuing the above experimental method, the experimental conditions are as follows: the front wheel steering angle is $\delta_f = 0$, the value range of braking torque is [830,880] N·m, the value interval is 10N·m, the initial value of longitudinal velocity is v_x = 42m/s, the initial value of lateral velocity is v_y = 4m/s, the initial value of yaw rate is ω = 0.25rad/s, and the simulation time is 15s. The phase space trajectories and phase trajectories onto the v_y-ω plane with different braking torques are shown in Fig. 9.

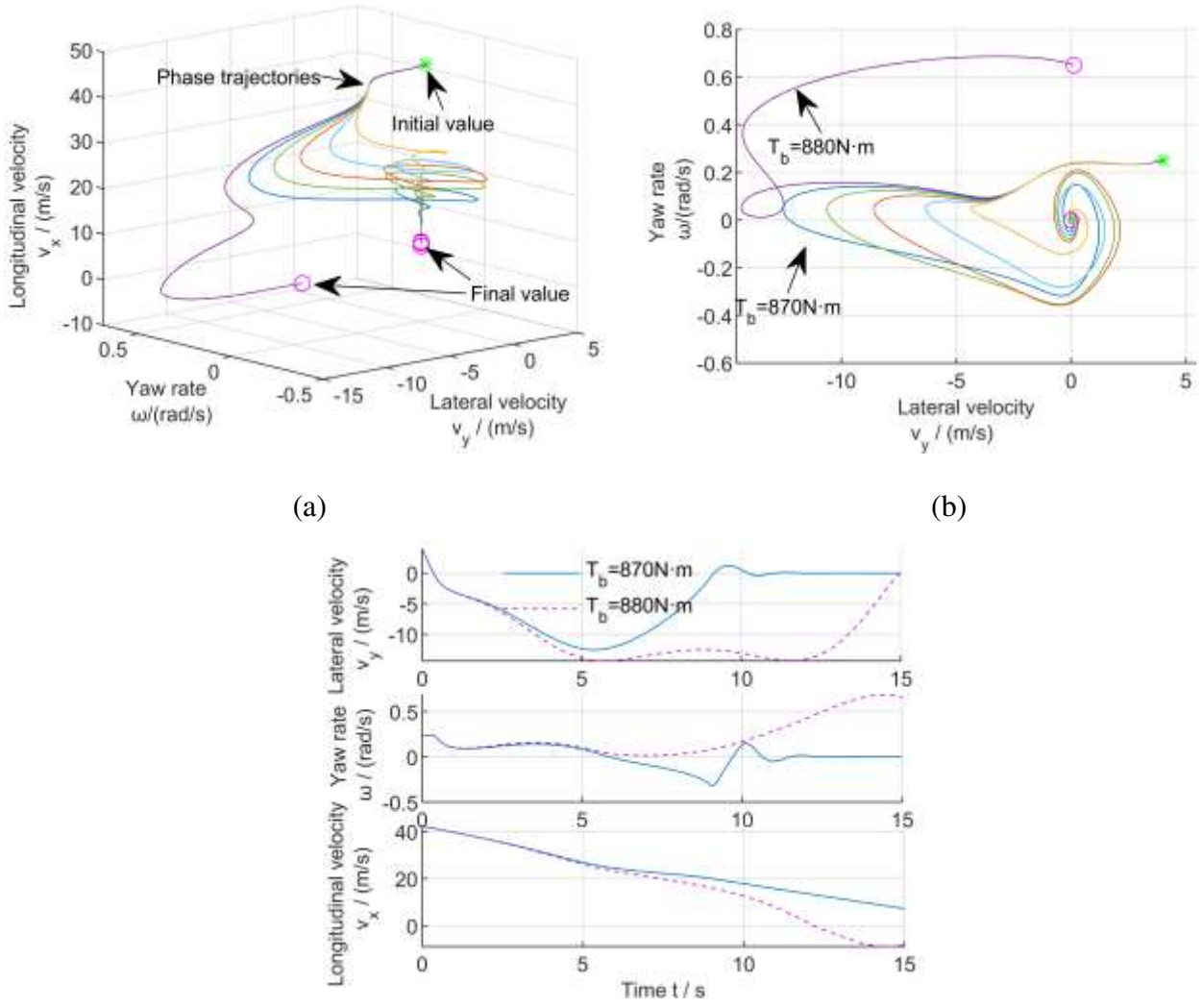

Fig. 9 Phase trajectories and time-domain responses of braking torques varying from 830N·m to 880N·m

The phase trajectories of the system change continuously with the increase of braking torque. When the braking torque increases from T_b = 870N·m to T_b = 880N·m, the phase trajectory of the system changes obviously in topology[23], that is, bifurcation occurs. From the time-domain response of state variables, it also can be seen that the nature of the system solution has also changed essentially.

Combined with the above analysis, the bifurcation diagram of the system state variable varying with the braking torque is calculated. The initial conditions of the system are as follows: the initial value of longitudinal velocity is v_x = 42m/s, the initial value of lateral velocity is v_y = 4m/s, and the initial value of yaw rate is ω = 0.25rad/s. Solve the 5DOF system equation, omit the beginning sampling cycles within the 20s of the simulation time, and sample the state variables according to a certain sampling frequency. The bifurcation diagram is shown in Fig. 10.

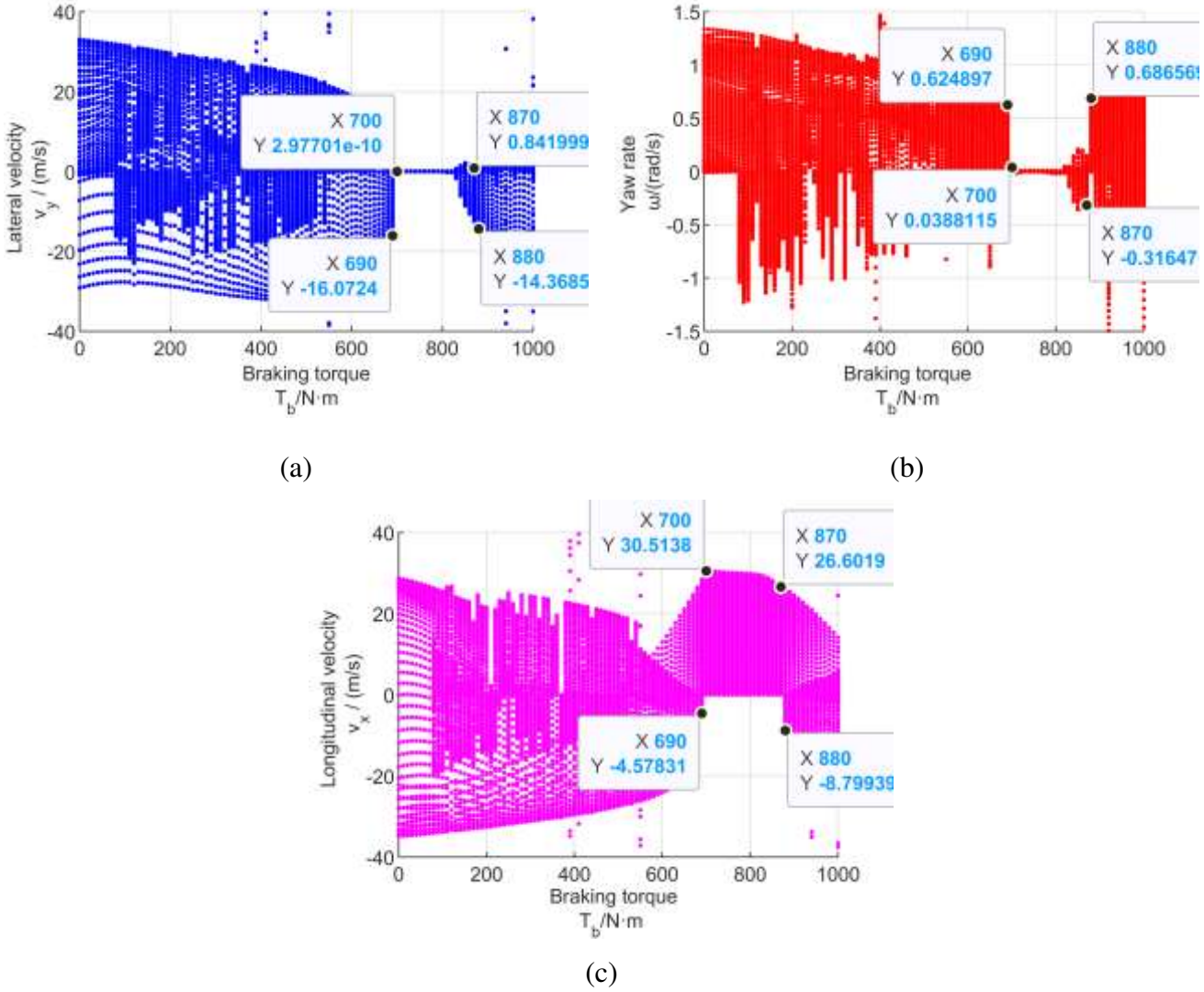

Fig. 10 Bifurcation diagram of state variables of vehicle lateral velocity, yaw velocity and longitudinal velocity(Omit the first 50 sampling cycles (one cycle is 0.1s) and the sampling frequency f = 10Hz)

Fig. 10 shows that when the braking torque is $T_b \leqslant$700N·m, the value range of lateral velocity v_y, yaw rate ω and longitudinal velocity v_x gradually decreases with the increase of braking torque. When the braking torque is T_b = 700N·m, the value range of lateral velocity v_y and yaw rate ω suddenly changes from [-16.07, 0.48] m/s and [0.01, 0.62] rad/s at T_b = 690N·m to [-0.21, 0.06] m/s and [-0.01, 0.04] rad/s. The value range of longitudinal velocity v_x suddenly changed from [-4.51, 28.44] m/s to [0.25, 30.51] m/s, from a positive and negative value range to a positive value range. When braking torque is T_b = 880N·m, the value range of lateral

velocity v_y and yaw rate ω changes from [-12.41, 1.18] m/s and [-0.32, 0.15] rad/s at T_b = 870N·m to [-14.37, 3.68] m/s and [-0.01, 0.69] rad/s. The value range of longitudinal velocity suddenly changed from [0,26.91] m/s to [-8.72,26.16] m/s, from a positive value range to a positive and negative value range.

To further judge the stability and dynamic bifurcation characteristics of the system, Fig. 11 calculates the Lyapunov exponent spectrum of the 5DOF when the braking torques are T_b = 690N·m, T_b = 700N·m, T_b = 870N·m and T_b = 880N·m.

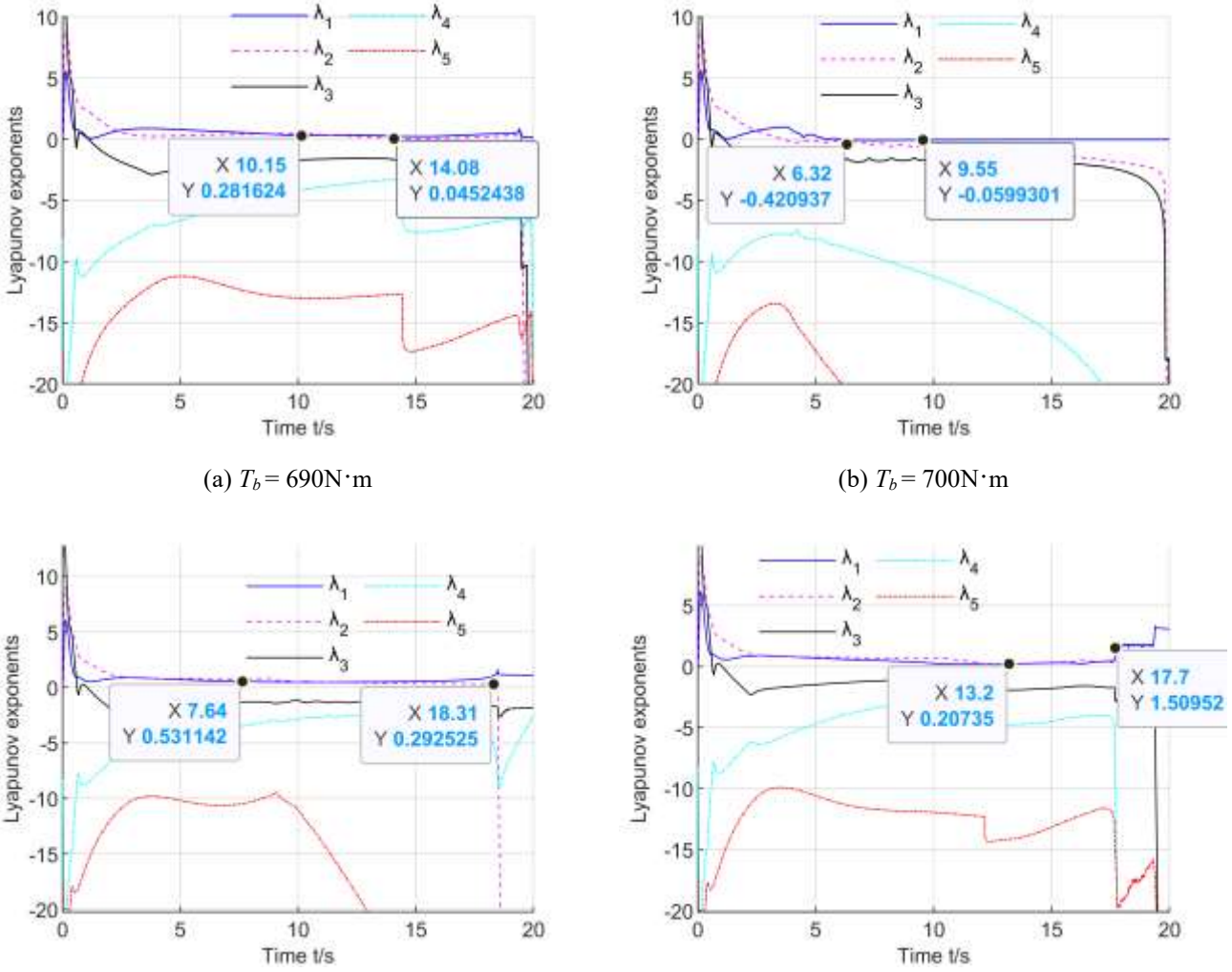

(a) T_b = 690N·m

(b) T_b = 700N·m

(c) T_b = 870N·m

(d) T_b = 880N·m

Fig. 11 Lyapunov exponent spectrum with different braking torques

When the braking torque is T_b = 690N·m, the Lyapunov exponent spectrum is (+, +, -, -,-), indicating that the system has hyperchaotic characteristics, while When the braking torque is T_b = 700N·m, the Lyapunov exponent spectrum is (-, -, -, -,-), indicating that the hyperchaotic characteristics of the system disappear; When the braking torque is T_b = 870N·m, the Lyapunov exponent spectrum is (+, +, -, -,-), indicating that the system has hyperchaotic characteristics; When the braking torque is T_b = 880N·m, the Lyapunov exponent spectrum is also (+, +, -, -, -), indicating that the hyperchaotic characteristics of the system still exist, and the maximum Lyapunov exponent continues to increase at the end of the simulation.

To sum up, when the braking torque T_b is in a specific interval [690,870] N·m, the system can recover from the unstable state to the controllable stable state. Excessive braking torque will not restore the stability of the system but will make the instability more severe (as can be seen from the comparison of the variation range of state variables in Fig. 9c and the Lyapunov exponent spectrum in Fig. 11). Based on the above analysis, it is speculated that under the input of zero front-wheel steering angle, the conjecture for the unstable vehicle to return to the stable state is that a specific range of braking torque must be applied.

4.2 Comparative validation

This section will calculate the bifurcation diagrams of the system state variables through the change of the vehicle's initial state variables input under zero front-wheel steering angle, and explore the relationship between the vehicle system stability and the braking torque range. The specific experimental conditions are shown in Table 6.

Table 6 Conjecture verification experimental conditions

Experimental groups	v_x （m/s）	v_y （m/s）	ω (rad/s)
Experimental 1	42	0	0
Experimental 2	42	4	0
Experimental 3	42	0	0.2
Experimental 4	42	8	0.4

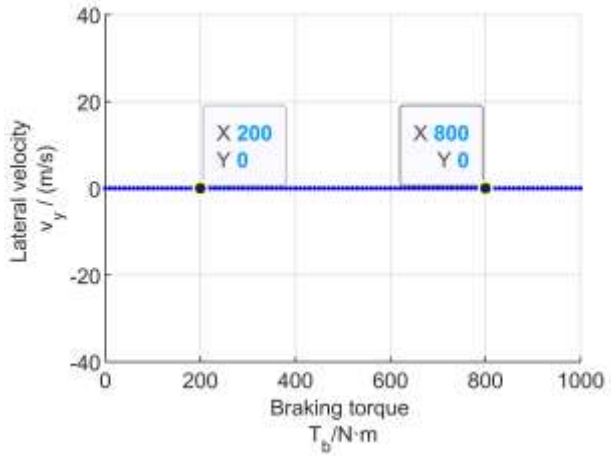

(a)

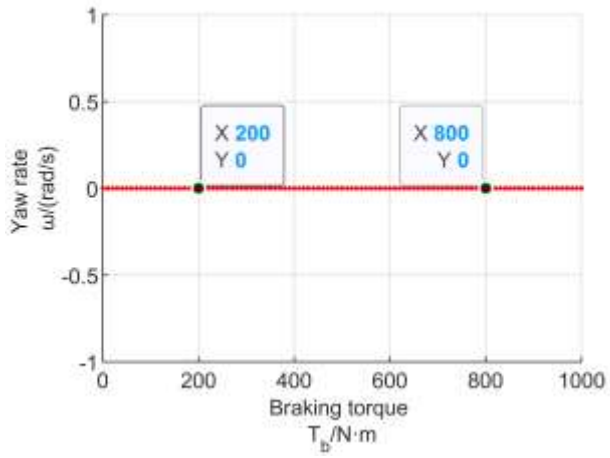

(b)

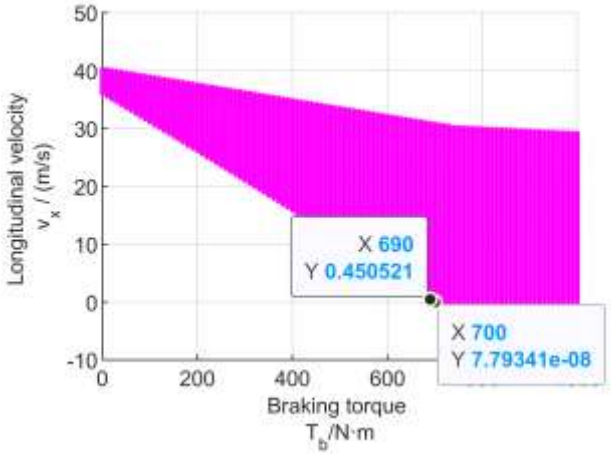

(c)

Fig. 12 Bifurcation diagram of experimental 1(Omit the first 50 sampling cycles (one cycle is 0.1s) and the sampling frequency f = 10Hz)

Fig. 12 is the bifurcation diagram of state variables under the input of experiment 1. Under the input of initial longitudinal velocity v_x = 42m/s, the system does not occur bifurcation. The value range of lateral velocity v_y and yaw rate ω is constant at 0, and the value range of longitudinal velocity v_x increases with the increase of braking torque, but the upper and lower limits of the value range are decreasing. When the braking torque is $T_b \geqslant 700$N·m, the minimum value of the longitudinal velocity range is 0, indicating that the vehicle finally reaches a stationary state.

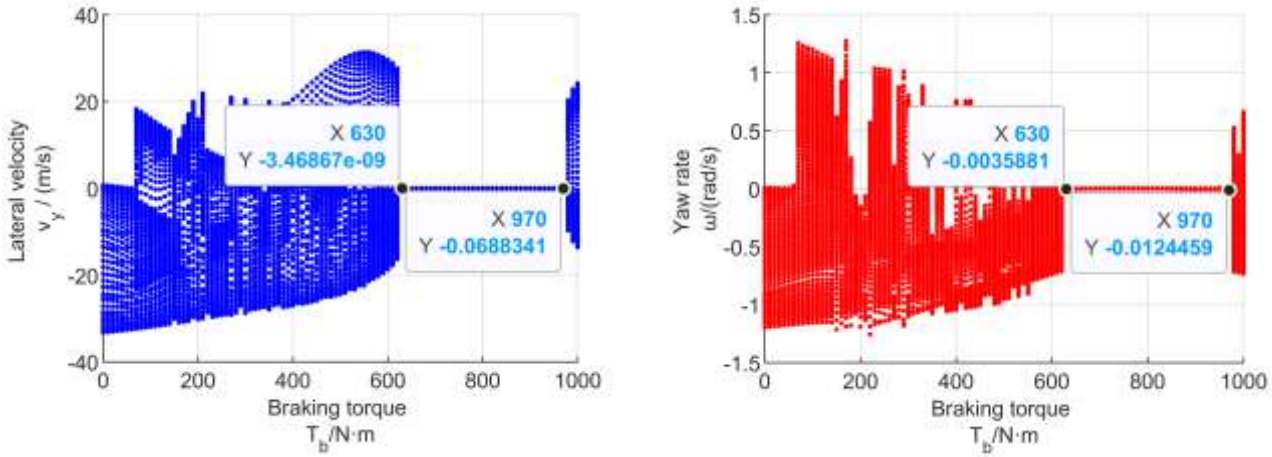

(a) (b)

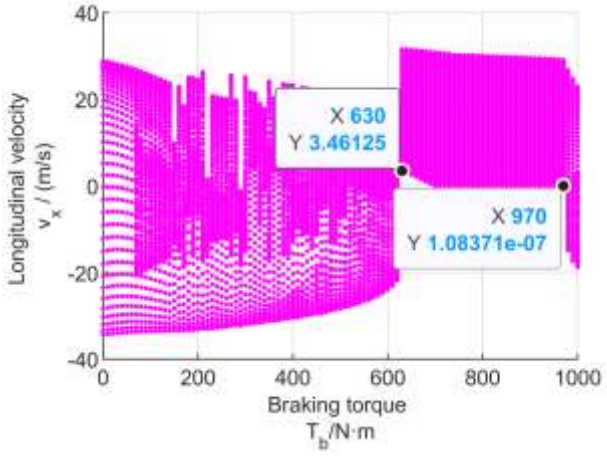

(c)

Fig. 13 Bifurcation diagram of experimental 2(Omit the first 50 sampling cycles (one cycle is 0.1s) and the sampling frequency f = 10Hz)

Fig. 13 shows the bifurcation diagram of state variables under the input of experiment 2. Compared with experiment 1, the input condition adds the input of lateral velocity v_y = 4m/s. It can be seen that there are bifurcations in the system, and the bifurcation phenomenon and analysis are similar to Fig. 10. Only when the braking torque T_b is applied in the [630, 970] N·m interval, the value range of lateral velocity v_y and yaw rate ω is small, and the value range of longitudinal velocity v_x is in the positive range, indicating that the unstable system has recovered to a stable state under braking.

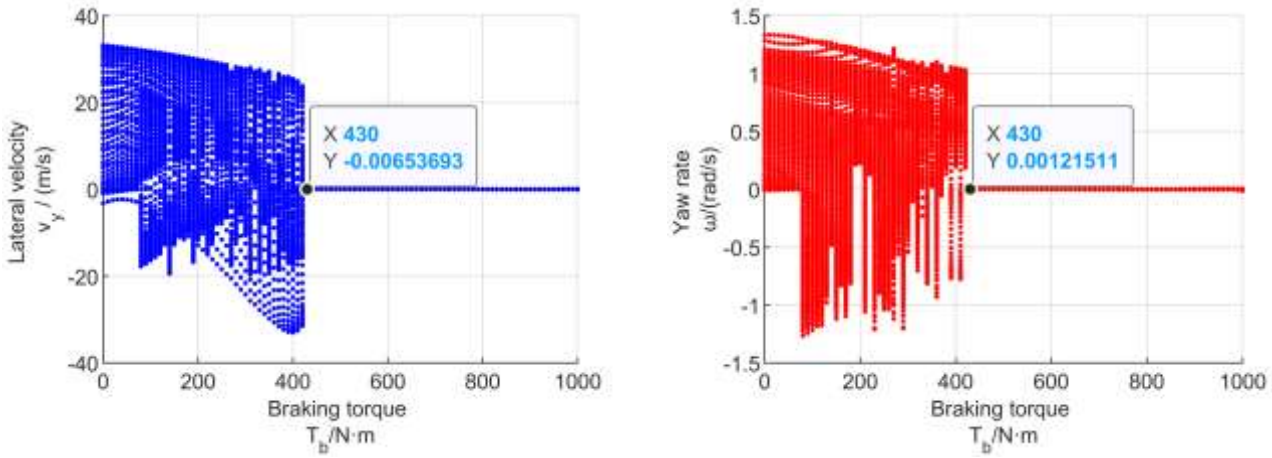

(a) (b)

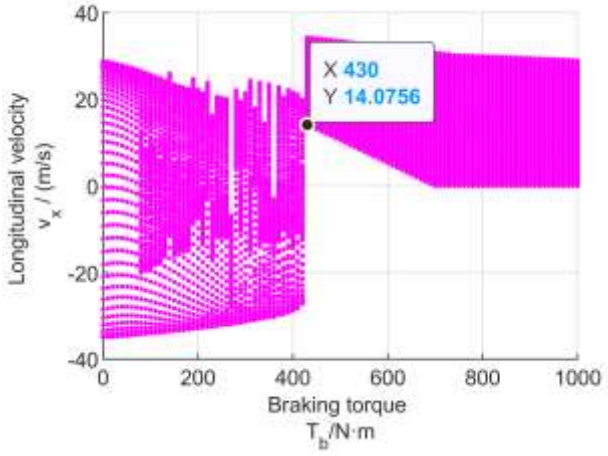

(c)

Fig. 14 Bifurcation diagram of experimental 3(Omit the first 50 sampling cycles (one cycle is 0.1s) and the sampling frequency f = 10Hz)

Fig. 14 shows the bifurcation diagram of state variables under the input of experiment 3. Compared with experiment 1, the input condition adds the input of yaw rate ω = 0.2rad/s. It can be seen that with the increase of braking torque, the value range of state variables is in a large range. When the braking torque is $T_b \geqslant 430$ N·m, the value range of lateral velocity v_y and yaw rate ω is small, and the value range of longitudinal velocity v_x is in the positive range, indicating that the instable system has recovered its stable state under braking.

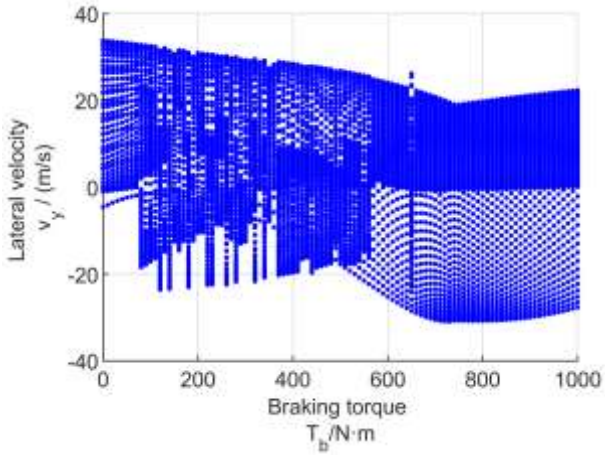

(a)

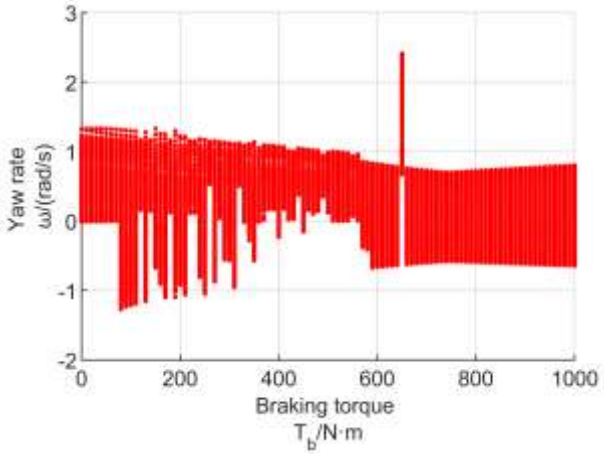

(b)

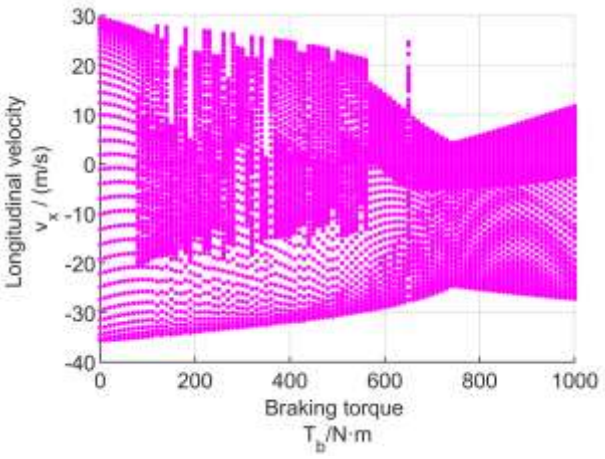

(c)

Fig. 15 Bifurcation diagrams of experimental 4(Omit the first 50 sampling cycles (one cycle is 0.1s) and the sampling frequency f = 10Hz)

Fig. 15 shows the bifurcation diagram of state variables under the input of experiment 4, the input conditions continue to add the input of lateral velocity v_y = 8m/s and yaw rate ω = 0.4 rad/s. The bifurcation diagram shows that the value range of state variables is in a large range, indicating that the system has been in a violent instability state. Under this initial condition, the instability of the system is too severe, and the application of braking torque cannot restore the system to a stable state.

5 Conclusion

(1) In this paper, the effect of braking torque on vehicle dynamic characteristics is studied by the nonlinear dynamic analysis method. The results show that the braking torque will directly affect the dynamic state and stability of the vehicle system.

(2) Taking the braking torque as the bifurcation parameter, the bifurcation characteristics of the 5DOF vehicle system are studied under the front wheel steering angle is 0. The results show that the braking torque can be regarded as the bifurcation parameter of the vehicle dynamics system, and multiple bifurcation phenomena may occur with the increase of braking torque.

(3) The chaotic characteristics of the 5DOF vehicle dynamic system are determined. The results indicate that hyperchaos may appear with braking torque increasing.

(4) The conjecture that a certain range of braking torque must be applied is put forward before a destabilized vehicle can return to the steady-state under zero front steering angle input, and is verified by the bifurcation diagram of state variables with different initial conditions.

The results show that the system will remain stable as the braking torque increases under initial stable conditions. Under some initial destabilization conditions, the system can only restore its steady-state within a certain range of braking torque. When the initial instability condition is increased to a certain extent, the change of braking torque will not restore the system to a stable state.

References

1. Sadri S., Wu C.: Stability analysis of a nonlinear vehicle model in-plane motion using the concept of Lyapunov exponents. Veh. Syst. Dyn. **51**(6),906-924(2013)
2. Flavio F., Michele R., Riccardo R., Mario T,. , Francesco T.: A combined use of phase plane and handling diagram method to study the effect of tyre and vehicle characteristics on stability. Veh. Syst. Dyn.**51**(8),1265-1285(2013)
3. Della Rossa, F., Gobbi, M., Mastinu, G., Piccardi, C., Previati, G.: Bifurcation analysis of a car and driver model. Veh. Syst. Dyn. **52**(sup1), 142–156 (2014)
4. Della Rossa, F., Mastinu, G.: Bifurcation analysis of an automobile model negotiating a curve. Veh. Syst. Dyn. **50**(10), 539-562 (2012)
5. Horiuchi S.: Evaluation of chassis control method through optimisation-based controllability region computation. Veh. Syst. Dyn. **50**(S1),19–31(2012)
6. Yi, J., Li, J., Lu, J., Liu, Z.: On the stability and agility of aggressive vehicle maneuvers: a pendulum-turn maneuver example. IEEE Trans. Control Syst. Technol. **20**(3), 663-676 (2012)
7. Liu L., Shi S., Shen S. and Chu J.: Vehicle planar motion stability study for tyres working in extremely nonlinear region. Chin J Mech Engng. **23**(2),185-194(2010)
8. Wang X., Shi S., Liu L., Jin L.: Analysis of driving mode effect on vehicle stability. INT J AUTO TECH-KOR.**14**(3),367-373 (2013)
9. Shi, S., Li, L., Wang, X., Liu, H., Wang, Y.: Analysis of the vehicle driving stability region based on the bifurcation of the driving torque and the steering angle. Proc. Inst. Mech. Eng. Part D J. Automob. Eng. **231**, 984-998 (2017)
10. Wang X., Shi S.: Vehicle coupled bifurcation analysis of steering angle and driving torque. Proc. Inst. Mech. Eng. Part D J. Automob. Eng. **235**(7), 1864-1875(2021)
11. Li L., Jia G., Chen J., Zhu H., Cao D., Song J.: A novel vehicle dynamics stability control algorithm based on the hierarchical strategy with constrain of nonlinear tyre forces. Veh. Syst. Dyn. **53**(8),1093–1116(2015)
12. Chen K., Pei X., Ma G.: Longitudinal/lateral stability analysis of vehicle motion in the nonlinear region. MATH PROBL ENG(2016)
13. Lu Q., Gentile P., Tota A., Sorniotti A., Gruber P., Costamagna F., De Smet, J.: Enhancing vehicle cornering limit through sideslip and yaw rate control. Mech Syst Signal Process. **75**(6),455-472(2016)
14. Della Rossa, F., Mastinu, G.: Straight ahead running of a nonlinear car and driver model-new nonlinear behaviours highlighted. Veh. Syst. Dyn. **56**(5), 753-768 (2018)
15. Mastinu G., Biggio D., Rossa F D.: Straight running stability of automobiles: experiments with a driving simulator. Nonlinear Dyn. **99**(4),2801-2818(2020)
16. Hossein M., Mehdi M., Sadra R.:A novel technique for optimal integration of active steering and differential braking with estimation to improve vehicle directional stability. ISA Trans. **80**,513-527(2018)
17. Carrie G., Bobier T., Craig E., John C., Rami Y., Hindiyeh J.: Christian Gerdes. Vehicle control synthesis using phase portraits of planar dynamics. Veh. Syst. Dyn. **57**(9),1-20(2019)
18. Steindl A., Edelmann J.,M Plöchl.: Limit cycles at oversteer vehicle. Nonlinear Dynamics, Nonlinear Dyn. **99**(2),313-321(2020)
19. Oh S., Avedisov S., Orosz G.:On the handling of automated vehicles: Modeling, bifurcation analysis, and experiments. Eur. J. Mech. A. Solids.**90**,(2021)
20. Xiong L., Yang X., Zhuo G., Leng B., Zhang R.: Review on Motion Control of Autonomous Vehicles. Chin J Mech Engng, **56**(10),127-143(2020)
21. Mu Y., Li L., Shi S.: Modified Tire-Slip-Angle Model for Chaotic Vehicle Steering Motion. Automotive Innovation, **1**(2):177-186(2018)

22. Pacejka, H.: Tire and Vehicle Dynamics. Elsevier, Amsterdam(2006)
23. Liu B.: Nonlinear Dynamics. Higher Education Press, Beijing(2004)

Funding

This work was partly supported by the National Natural Science Foundation of China (grant number 52175497).

Competing Interests

The authors have no relevant financial or non-financial interests to disclose.

Author Contributions

All authors contributed to the study conception and design. Material preparation, data collection and analysis were performed by Xianbin Wang, Weifeng Li and Zhipeng Li. The first draft of the manuscript was written by Xianbin Wang and all authors commented on previous versions of the manuscript. All authors read and approved the final manuscript.

Data Availability

The datasets generated during and/or analysed during the current study are not publicly available due to simulation experiments but are available from the corresponding author on reasonable request.